Structural and electronic properties of the Au(001)/Fe(001) interface from density functional theory calculations

Magali Benoit[*]

CEMES-CNRS UPR 8011, 29 rue Jeanne Marvig, 31055 Toulouse Cedex, France

Cyril Langlois[†]

Laboratory for Materials and Quantum Phenomena, CNRS University Paris Diderot, Paris 7, 4 rue Elsa Morante, 75013 Paris, France

Nicolas Combe, Hao Tang, and Marie-José Casanove

CEMES-CNRS UPR 8011, 29 rue Jeanne Marvig, 31055 Toulouse Cedex, France

A density functional theory (DFT) investigation of the structural and electronic properties of the Au(001)/Fe(001) interface, as a function of the number of Au layers deposited on the Fe substrate (from 1 to 11 Au monolayers), is presented. The elastic effects on the interface properties due to the lattice mismatch between Fe and Au, calculated by DFT using the generalized gradient approximation, are also evaluated. At the interface, the interlayer distances in the Fe substrate as well as in the Au slab expand. The Fe atoms of the interface exhibit an enhanced magnetic moment and the Au atoms of the interface bear a nonzero (but very low) magnetic moment. The calculated interface energy favors the formation of core-shell Fe@Au nanoparticles, where Au(001) is in epitaxy at 45° on (001) facets of a Fe nanocube. Finally, the analysis of the electronic properties shows that the work of adhesion of the interface is maximum for a coating of Fe with 2 Au monolayers, which can be explained by a strong overlap between the electronic densities of the Fe interface atoms with those of the Au surface atoms.

PACS number(s): 71.15.Mb, 68.35.bd, 61.46.Df

I. INTRODUCTION

Magnetic nanoparticles play an important role in a wide number of applications from ferrofluids to data storage and catalysis, as well as in biomedicine. In this particular domain, magnetic nanoparticles are used for medical imaging, drug delivery, cancer therapy, etc. The properties of nanoparticles can be tuned by reducing their size and the possibility of controlling at the same time their size, shape, and composition provides great flexibility for their different biomedical applications.[1–3]

However, these particles cannot be used as such: They are usually not biocompatible and they can easily be oxidized, which can weaken their magnetic properties. One possible solution for using magnetic particles in biomedical applications is to passivate their surface with an inert and biocompatible metal. Gold has been recognized as being biocompatible and chemically inert and it presents functionalities with several enzymes.[4] The fabrication of core-shell nanoparticles with a magnetic core and a shell made of gold has then become a promising route for biomedical applications. Nevertheless, important questions remain to be addressed: Is the coating of magnetic nanoparticles by gold easily achievable? To what extent does this coating modify the magnetic properties of the core? And does it really prevent core oxidation?

In the last decade, there have been some experimental investigations in this direction with several tentative synthesis of Fe@Au core-shell nanoparticles. Most of the gold-coated iron nanoparticles were synthesized following a chemical protocol such as the reverse micelles method and presented either an oxidized core (Fe_2O_3 or Fe_3O_4)[1,3,5] or a pure iron core.[6–12] FeAu alloy nanoparticles have also been synthesized using pulse laser deposition,[13] electron beam evaporation,[14] and reverse micelles encapsulation.[15]

The structure and the morphology of core-shell nanoparticles depend on many different fabrication parameters but also on the intrinsic characteristics of the two metals brought together. In particular, the differences between the surface energies and the value of the interface energies between the two metals play an important role for nanoparticle growth. Unfortunately, the values of the interface and surface energies are extremely difficult (if not impossible) to measure experimentally. There is therefore an increasing demand for simulations of realistic models, likely to bring valuable information on these parameters.

Recently, we succeeded in growing core-shell Fe@Au nanoparticles of 8–10 nm using UHV magnetron sputtering[16] (Fig. 1). These particles take, for most, a very unusual morphology in which bcc iron nanocubes are surrounded by truncated pyramids of fcc gold on every cube facet. The cube facets are Fe(001) coated by Au(001) with an epitaxial relationship between Au(001) and Fe(001) at 45° in the (001) plane, i.e., Au(001)[100]/Fe(001)[110].

Modeling these nanoparticles, a few nanometres wide, would be computationally accessible only using very simple and fast-computing atomic interaction models such as embedded atom models (EAMs) for instance. In order to precisely characterize the structural magnetic and electronic properties of the observed Fe@Au nanoparticles, density functional theory (DFT) was here used for the study of the Au(001)/Fe(001) interface. To our knowledge, this interface has never been studied as such, even if calculations of Fe_mAu_n multilayers of the same orientation[17,18] or small $Fe_n@Au_m$ nanoclusters[19] exist.

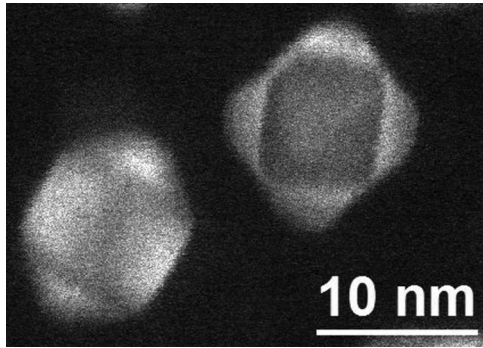FIG. 1. Transmission electron microscopy image of two differently oriented Fe@Au nanoparticles (left: $[110]_{Fe}$ orientation; right: $[001]_{Fe}$ orientation) grown in Al_2O_3 by UHV magnetron sputtering.

In this paper, structural, magnetic, and electronic properties of the Au(001)/Fe(001) interface, made of a substrate of Fe(001) on which Au is deposited, are carefully investigated as a model for the experimentally observed Fe@Au nanoparticles. The interface is first described and the simulation details are given in Sec. II A. The structural and magnetic properties of the pure Fe and pure Au bulks and slabs are then analyzed in detail in Secs. III and IV. These studies provide a reference for the study of the interface, which is done in Sec. V. Especially, the effect of the number of monolayers (MLs) in the Au slab is investigated, starting from a single layer up to 11 layers ($\approx$23 Å thick).

II. DETAILS OF THE CALCULATIONS

A. Model of the Au(001)/Fe(001) interface

The interface between Fe(001) and Au(001) is modeled as several fcc Au MLs deposited on a substrate of bcc Fe, which is made of 10 layers. The choice of the number of Fe layers for the substrate is justified in Sec. IV. The atoms of the two bottom layers of the iron slab are fixed to the bulk positions in order to mimic an infinite substrate. The epitaxial relationship between Au(001) and Fe(001) is at 45 $^\circ$ in the (001) plane: The atoms of the Au layers are positioned on top of the Fe atoms as depicted in Fig. 2.
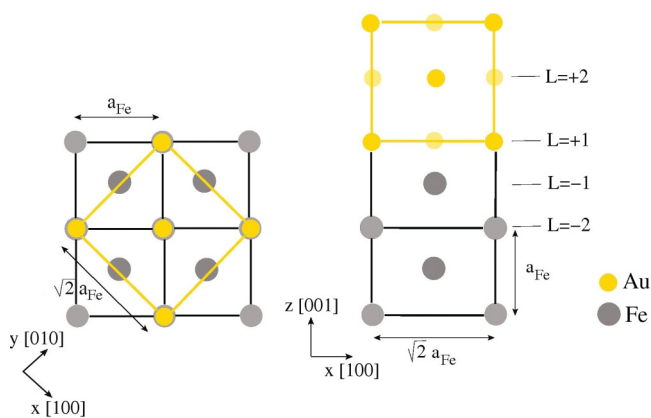

FIG. 2. (Color online) Sketch of the Au/Fe(001) interface model. Gray and yellow balls are Fe and Au atoms, respectively. The L values indicate the index of the layer in the interface model.

The lattice parameter of the Fe crystal in the [100] and [010] directions is fixed to the equilibrium lattice constant of α-Fe (see Table I). For this geometry, the mismatch between Fe(001) and Au(001) is defined as

$$m_{Au/Fe} = (a_{Au} - \sqrt{2}a_{Fe})/\sqrt{2}a_{Fe}, \qquad (1)$$

where a_{Au} and a_{Fe} are the equilibrium lattice parameters of Au and Fe. For the simulation of the interface, systems with a number of Au layers ranging from 1 to 11 MLs were simulated using periodic boundary conditions with an empty space of at least 9 Å above the free Au surface in the [001] direction. Initially, the distance between the Au slab and the Fe slab was taken to be equal to the iron interlayer spacing in the [001] direction. All the atoms were allowed to relax except for the two bottom layers of the iron slab, which were kept at their bulk positions.

B. Details of the DFT simulations

Density functional theory calculations[20] were performed in the Perdew-Burke-Ernzerhof (PBE) generalized gradient approximation (GGA) for the exchange and correlation energy, using the VASP simulation package[21] in a periodic simulation cell. The PBE functional is known to give results in good agreement with experimental data for bulk Fe, in particular regarding the bulk magnetic properties.[22] In contrast, the bulk properties of Au are better reproduced using the local-density approximation (LDA) functional.[23] Since the present study deals with the interface between Fe and Au, and given the fact that the magnetic ground state of iron cannot be found using LDA,[24] the PBE functional was adopted in our calculations. Nevertheless, when possible, the errors made between the PBE and LDA functionals were estimated.

The simulations were performed using Projector Augmented-Wave pseudopotentials with the 3d and 4s electrons as valence electrons for α-Fe and with the 5d and 6s electrons as valence electrons for Au. Cutoff energies of 450 eV for iron, 600 eV for gold, and 600 eV for the interface were necessary to achieve convergence of the results with respect to the plane-wave basis set. A Gaussian broadening was used with a smearing of 0.01 eV for the electron occupation. For all calculations, a Monkhorst-Pack mesh of k points was employed to sample the Brillouin zone. For bulk calculations, a mesh of $20 \times 20 \times 20$ was used for bcc Fe and a mesh of $12 \times 12 \times 12$ was used for fcc Au. For the Fe(001) surface calculations, a mesh of $20 \times 20 \times 1$ was used; however, for the Au(001)/Fe(001) interface calculations and for the (001)Au surface calculation, a mesh of only $12 \times 12 \times 1$ was sufficient to reach convergence.

For the α-Fe bulk and surface, and for the (001)Au/(001)Fe interface, spin-polarized calculations were carried out.

III. BULK PROPERTIES

Table I reports the lattice parameters, some elastic constants, and the magnetic properties for bulk α-Fe and fcc Au. For α-Fe, the results are in very good agreement with experiments and with recent DFT calculations performed in the PBE or Perdew and Wang approximation.[22–24,31] In contrast, the results obtained for Au with the PBE functional show

TABLE I. Bulk properties of bcc α-Fe and fcc Au, computed in DFT-PBE and compared to experiments (Expt.) when possible.

	Fe		Au	
	DFT-PBE	Expt.	DFT-PBE	Expt.
a [Å]	2.835	2.866[23]	4.174	4.08,[25] 4.079[23,26]
B [GPa]	185	165,[23] 168,[25] 168–172[27]	135	162–180,[26] 167,[23] 180[28]
C_{21} [GPa]	144	130–136,[29] 136[25]	117	163–175,[26] 170[28,30]
C_{11} [GPa]	267	226–232,[29] 232[25]	171	192–209,[26] 202[28,30]
μ [μ_B/atom]	2.21	2.22[25]	—	—

significant deviations from the experimental values of $+2.3\%$ for the lattice parameter, -19% for the bulk modulus and -31% and -14% for the C_{21} and C_{11} elastic constants, respectively. This overestimation of the lattice parameter and underestimation of the elastic properties by the PBE functional have already been referenced.[32] Because of the overestimation of the Au lattice constant, the mismatch $m_{\text{Au/Fe}}$ between Fe(001) and Au(001) is found to be equal to $+4.11\%$ using the PBE functional whereas it is equal to $+0.66\%$ experimentally. This discrepancy between the experimental and PBE mismatch will be discussed in the calculation of the surface and interface properties.

IV. SURFACE PROPERTIES

The surface properties of Fe(001) and Au(001) were investigated using a slab geometry with two free surfaces and an empty space of at least 10 Å between slabs. The convergence of the surface energies, of the interlayer distances, and of the atomic magnetic moments was studied as a function of the slab thickness (number of atomic layers, N).

The surface energy γ_{001} is defined from the surface excess energy E_{surf}^N per unit area:

$$E_{\text{slab}}^N = 2E_{\text{surf}}^N A + N n_{at} E_{\text{bulk}}, \qquad (2)$$

$$\gamma_{001} = \lim_{N \to \infty} E_{\text{surf}}^N = \lim_{N \to \infty} \frac{E_{\text{slab}}^N - N n_{at} E_{\text{bulk}}}{2A}, \qquad (3)$$

where N is the number of layers in the slab, E_{bulk} is the bulk atomic energy at equilibrium, A is the surface area at equilibrium, and E_{slab}^N is the total energy of a slab of N atomic layers with n_{at} atoms each. The surface excess energy per
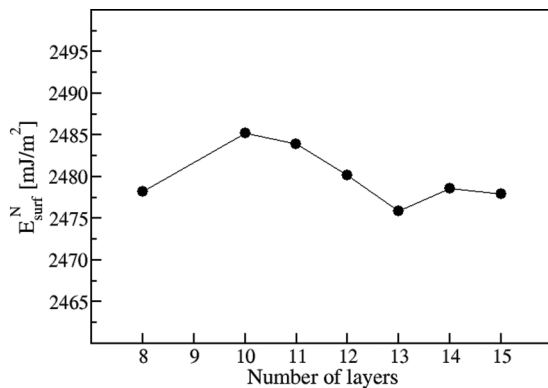

FIG. 3. Surface excess energy per unit area as a function of the number of layers in the slab for the Fe(001) surface.

unit area, E_{surf}^N, converges to the surface energy γ_{001} when the number of layers, N, tends to infinity. E_{surf}^N gives a good estimation of γ_{001} provided that N is large enough (see below) and that the bulk and slab calculations are carried out with the same level of accuracy (number of k points, cutoff energy, and pseudopotentials).[32]

A. Fe(001) surface

Figure 3 reports the Fe(001) surface excess energy per unit area, E_{surf}^N, as a function of the number of layers in the slab. The surface energy E_{surf}^N converges to a value of about $\gamma_{001} = 2478$ mJ/m^2. This estimation is in very good agreement with the experimental values of 2417,[33] 2475,[34] and 2550 mJ/m^2 (Ref. 35) (Table II) determined using liquid surface tension measurements and extrapolating the data to 0 K to give a numerical value for the solid.

After relaxation of the slab, the interlayer distances are modified with respect to the bulk interlayer distances. In Fig. 4, the deviation of the interlayer distances with respect to the bulk value, given by $(d_{i,i+1} - d_{\text{bulk}}^{\text{Fe}})/d_{\text{bulk}}^{\text{Fe}}$ where $d_{\text{bulk}}^{\text{Fe}} = a_{\text{Fe}}/2$, are presented as a function of the number of layers. $d_{i,i+1}$ is the interlayer distance between two adjacent layers i and $i+1$, the index of the layer in the slab being numbered starting from the surface. In Fig. 4, the interlayer distances softly depend on the number of layers in the slabs: They are approximately converged for slabs with a number of layers at least equal to 10. The first interlayer distance d_{12} is found to contract by -2.2% while the second one d_{23} expands by $+3.2\%$. The influence of the surface is no longer visible beyond the fourth layer under the surface; i.e., the interlayer distance d_{45} does not differ from the bulk value. These results are in very good agreement with previous calculations carried out on the Fe surfaces using DFT with different functionals.[36–39]

The effect of the surface on the atomic magnetic moment is also investigated: Figure 5 reports the magnetic moment per atom in each layer as a function of the number of layers in the slab. The atomic magnetic moments converge for slabs with a number of layers at least equal to 10. For slabs containing

TABLE II. Surface energies computed in DFT-PBE and DFT-LDA for the different investigated surfaces, in mJ/m^2.

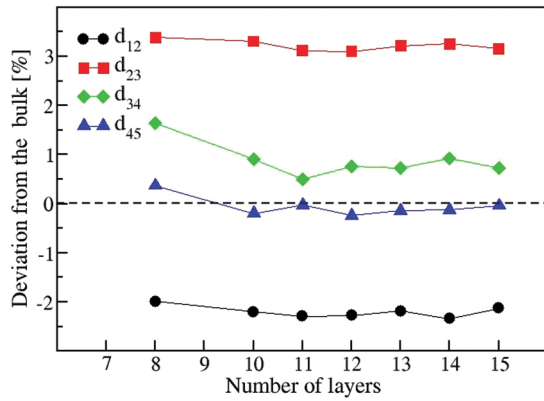|	DFT-PBE	DFT-LDA	Expt.
Fe γ_{001}	2478	—	2417,[33] 2475,[34] 2550[35]
Au γ_{001}	873	1329	—
Au γ_{111}	734	1020	1500[33]

FIG. 4. (Color online) Relaxation of the interlayer distances (as a percentage of the bulk interlayer spacing) as a function of the number of layers in the Fe(001) slab. The symbols correspond to the different interlayer distances indexed as $d_{i,i+1}$, i and $i+1$ being the positions of the layer in the slab, starting from the surface.

more layers, the Fe atoms of the surface layer (first layer), of the subsurface layer (second layer), and of the subsubsurface layer (third layer) have, respectively, magnetic moments of 2.94, ≈ 2.36, and ≈ 2.41 μ_B/atom, in very good agreement with previous DFT results.[36,38] From the fourth sublayer, the magnetic moment recovers its bulk value of 2.21 μ_B/atom. This strong enhancement of the magnetic moment is due to the reduced coordination of surface atoms.

The atomic magnetic moment, as well as the interlayer distance, converges when a 10-layer Fe slab is used. A 10-layer Fe slab is thus sufficient to get fairly accurate results regarding the structural properties and will therefore be used for the interface model.

B. Au(001) surface

Following the work done for the Fe(001) surface, Fig. 6 reports the surface excess energy E^N_{surf} per unit area for the Au(001) surface as a function of the number of layers in the Au slab. E^N_{surf} shows some damped oscillations as a function of N centered around the value of 873 mJ/m^2, which gives a fair estimation of the surface energy $\gamma_{001} = 873$ mJ/m^2. This value is in good agreement with previous DFT results using GGA
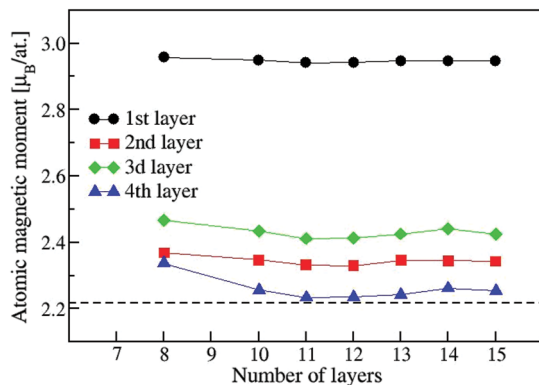

FIG. 5. (Color online) Evolution of the atomic magnetic moment as a function of the number of layers in the Fe(001) slab. The different symbols correspond to atoms in different layers and the dashed line gives the bulk value.
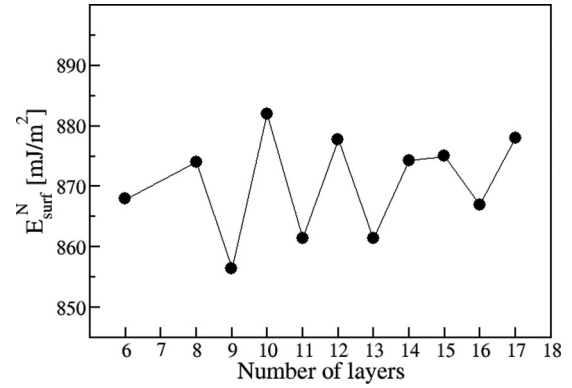

FIG. 6. Surface excess energy per unit area as a function of the number of layers in the slab for the Au(001) surface.

functionals[32,40,41] but is much underestimated compared to the experimental value of 1500 mJ/m^2 for the Au (111) surface.[33] Since the (001) surface is known to be less energetically favorable than the (111) surface, its surface energy should be even higher than 1500 mJ/m^2. Using the LDA functional, the estimation for the Au (001) surface energy (≈ 1330 mJ/m^2) is closer (although still lower) to the expected experimental value (Table II). Similar calculations using the PBE functional performed on a 17-layer Au(111) slab yield a surface energy of $\gamma_{111} = 734$ mJ/m^2, which is slightly smaller than the Au(001) surface energy, in agreement with previous calculations.[32,40,41] The results for the surface energies of α-Fe and fcc Au are summarized in Table II.

For the Au(001) surface, the structure of the slab in analyzed in Fig. 7, where the deviation of the interlayer distances with respect to the bulk value, $(d_{i,i+1} - d^{\text{Au}}_{\text{bulk}})/d^{\text{Au}}_{\text{bulk}}$ where $d^{\text{Au}}_{\text{bulk}} = a_{\text{Au}}/2$, are presented as a function of the number of layers in the Au slab. Significant oscillations in the interlayer spacing can be observed; these tend to decrease with increasing number of layers: The values of interlayer distances converge. Once converged, the first interlayer distance d_{12} undergoes a contraction of $\approx -1.5\%$ while the interlayer spacing underneath d_{23} remains unchanged. Similarly to the case of Fe, the number of layers in the Au slab seems to play
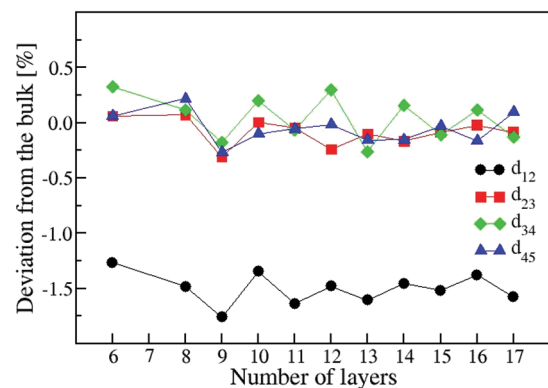

FIG. 7. (Color online) Relaxation of the interlayer distances (as a percentage of the bulk interlayer spacing) as a function of the number of layers in the Au(001) slab. The symbols correspond to the different interlayer distances indexed as $d_{i,i+1}$, i and $i+1$ being the positions of the layer in the slab, starting from the surface.

an important role up to a minimum of 11 layers. These results are in very good agreement with previous calculations of the (001)Au surface relaxation using GGA functionals.[32,40,41] Note that the surface reconstructions are not considered here, which prevents us from being able to make a direct comparison of the obtained values with experiments.

C. Strained Au(001) surface

In order to better evaluate the effect of the PBE lattice mismatch on the Au slab energy and on the Au surface energy, an 11-layer Au slab was relaxed for different values of the isotropic strain in the xy plane, $\epsilon_{xx} = \epsilon_{yy}$. In the Au(001)/Fe(001) system, equal ϵ_{xx} and ϵ_{yy} strains applied to the Au slab are induced by the lattice mismatch:

$$\epsilon_{xx} = \epsilon_{yy} = \frac{\sqrt{2}a_{\mathrm{Fe}} - a_{\mathrm{Au}}}{a_{\mathrm{Au}}}.$$

In the present DFT-PBE calculations, $\epsilon_{xx}^{\mathrm{PBE}} = -3.95\%$ whereas $\epsilon_{xx}^0 = -0.66\%$ experimentally. The energy of a Au slab subject to strains in the x and y directions reads

$$E_{\mathrm{slab}}^N(\epsilon_{xx},\epsilon_{yy}) = Nn_{at}E_{\mathrm{bulk}}^0 + 2\gamma_{001}A \\ + u_{el}V + 2\sigma_{001}^{xx}A\epsilon_{xx} + 2\sigma_{001}^{yy}A\epsilon_{yy}, \quad (4)$$

where the first two terms are the bulk and surface excess free energy terms (which converge for a 11-layer slab) of the unstrained slab ($\epsilon_{xx} = 0$). The next two terms are the bulk and surface excess elastic energy:[42] u_{el} is the elastic energy per unit volume, V is the volume at equilibrium, σ_{001}^{xx} and σ_{001}^{yy} are the surface stress in the x and y directions, respectively, and A is the reference surface area. Since, both x and y directions are equivalent, $\sigma_{001}^{xx} = \sigma_{001}^{yy} = \sigma_{001}$. For an fcc Au slab, whose strains $\epsilon_{xx} = \epsilon_{yy}$ are imposed, the elastic energy per unit volume reads

$$u_{el} = (C_{11} + C_{12})\epsilon_{xx}^2 + \frac{1}{2}C_{11}\epsilon_{zz}^2 + 2C_{12}\epsilon_{xx}\epsilon_{zz}, \quad (5)$$

where C_{12} and C_{11} are the elastic constants reported in Table I. Introducing Eq. (5) into Eq. (4) and minimizing the latter with respect to ϵ_{zz} gives

$$\epsilon_{zz} = \frac{-2C_{12}}{C_{11}}\epsilon_{xx}. \quad (6)$$

The total energy of the slab can thus be written as a function of ϵ_{xx}:

$$E_{\mathrm{slab}}^N(\epsilon_{xx}) = Nn_{at}E_{\mathrm{bulk}}^0 + 2\gamma_{001}A + \left[C_{11} + C_{12} - 2\frac{C_{12}^2}{C_{11}}\right]V\epsilon_{xx}^2 \\ + 4\sigma_{001}A\epsilon_{xx} \quad (7)$$

and it is then minimum for

$$\epsilon_{xx}^{\min} = \frac{-2\sigma_{001}A}{\left[C_{11} + C_{12} - 2\frac{C_{12}^2}{C_{11}}\right]V}. \quad (8)$$

The value of $\epsilon_{xx}^{\min}$ at which $E_{\mathrm{slab}}^N(\epsilon_{xx})$ is minimum therefore depends on the number of layers in the Au slab, through the A/V term, and should tend toward 0 for an infinite number of layers. For instance, the calculated total energy $E_{\mathrm{slab}}^N(\epsilon_{xx})$ of the 11-layer Au slab as a function of ϵ_{xx} is parabolic and is minimum for a strain in the xy plane of $\epsilon_{xx}^{\min} = \epsilon_{yy}^{\min} \approx -1.77\%$. It is possible to evaluate the surface stress σ_{001} by
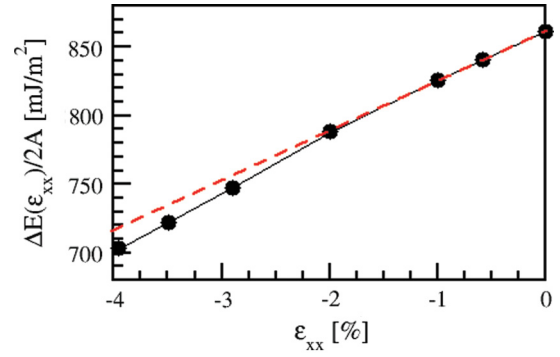

FIG. 8. (Color online) Energy difference between the Au bulk energy and the Au slab energy for an isotropic strain in the xy plane ϵ_{xx} (black circles). The red line shows a linear fit of the points at small deformations ($|\epsilon_{xx}| \leqslant 2\%$).

computing the difference $\Delta E(\epsilon_{xx})$ between the total energy of the slab, $E_{\mathrm{slab}}^N(\epsilon_{xx})$, and the bulk atomic energy, $E_{\mathrm{bulk}}(\epsilon_{xx})$, subject to the same contraction in the xy plane and relaxed along the z direction [001]:

$$\Delta E(\epsilon_{xx}) = E_{\mathrm{slab}}^N(\epsilon_{xx}) - Nn_{at}E_{\mathrm{bulk}}(\epsilon_{xx}) \\ = 2\gamma_{001}A + 4\sigma_{001}A\epsilon_{xx}, \quad (9)$$

with

$$E_{\mathrm{bulk}}(\epsilon_{xx}) = E_{\mathrm{bulk}} + u_{el}V_{at} \\ = E_{\mathrm{bulk}} + \left[C_{11} + C_{12} - 2\frac{C_{12}^2}{C_{11}}\right]V_{at}\epsilon_{xx}^2, \quad (10)$$

where $V_{at} = V/(Nn_{at})$ is the equilibrium bulk atomic volume.

Figure 8 reports the variation of $\Delta E(\epsilon_{xx})$ per unit area as a function of ϵ_{xx} for an Au slab of 11 layers. For small deformations ($|\epsilon_{xx}| \leqslant 2\%$), the energy difference $\Delta E(\epsilon_{xx})$ is a linear function of ϵ_{xx}: The slope and y intercept are, respectively, proportional to the surface stress σ_{001} and to the surface energy γ_{001}. The nonlinearity of $\Delta E(\epsilon_{xx})/2A$ as a function of ϵ_{xx} for $|\epsilon_{xx}| \geqslant 2\%$ is related to the existence of a surface stiffness tensor. The determination of this surface stiffness tensor is out of the scope of this study. The red dashed line in Fig. 8 corresponds to a linear fit of $\Delta E(\epsilon_{xx})/2A$ for small values of ϵ_{xx}, from which a value of $\sigma_{001} \approx 1.836$ J/m^2 (114.6 meV/Å^2) can be deduced. This value should be compared to values from the literature: 2.723 J/m^2 (LDA),[43] 2.073 J/m^2 (PBE),[41] and 3.53 J/m^2 (LDA).[44] The difference between the present value and those of previous DFT works comes essentially from the use of a different functional or, if the same functional is used, from the fact that the bulk energy in Ref. 41 was not obtained from a fully relaxed bulk system at each ϵ_{xx} deformation. The positive value of the surface stress σ_{001} is consistent with the negative value of the bulk strain field $\epsilon_{xx}^{\min} \approx -1.77\%$ deduced from Eq. (7). Note that due to the computational cost of these calculations, the study of the convergence of σ_{001} as a function of the number of layers, N, in the slab was not carried out.

Using this value, the surface excess elastic energy $4\sigma_{001} \times \epsilon_{xx}$ per unit area can be estimated for the strain field corresponding to the experimental mismatch between Fe(001) and Au(001) ($\epsilon_{xx}^0 = -0.66\%$) and the one corresponding to the PBE mismatch ($\epsilon_{xx}^{\mathrm{PBE}} = -3.95\%$). For ϵ_{xx}^0, the surface excess
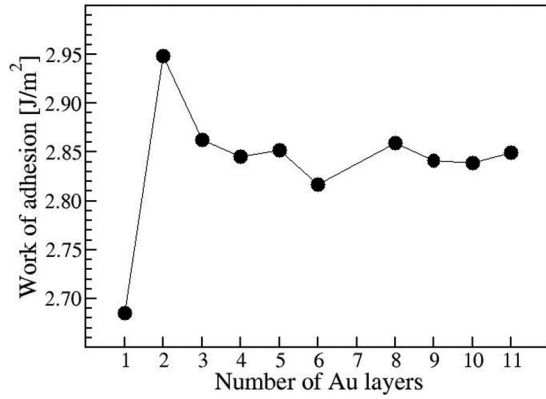
FIG. 9. Evolution of the work of adhesion of Au(001) on Fe(001) as a function of the number of Au layers.

elastic energy per unit area is approximately 12.1 mJ/m^2 whereas, for ϵ_{xx}^{PBE}, it is $\approx$72.5 mJ/m^2. The difference between these two values, $\approx$60.4 mJ/m^2, gives an estimation of the error made on the surface elastic energy of a strained Au slab due to the difference between the experimental and the PBE mismatch.

V. Au(001)/Fe(001) INTERFACE

The Au(001)/Fe(001) interface system is built as described in Sec. II A and its properties are analyzed as a function of the number of Au(001) MLs deposited on the Fe(001) substrate.

A. Work of adhesion

In this section, the work of adhesion, W_{ad}, of the Au(001) slab onto the Fe(001) substrate is estimated: It is the energy required (per unit area) to reversibly separate a material into two free surfaces. Attractive interaction between two surfaces corresponds to a positive W_{ad}. It can be calculated by subtracting the corresponding energy of Fe(001) and Au(001) slabs computed in the same conditions (i.e., the same number of layers, the same energy cutoff and the same number of k points):[45]

$$W_{ad} = [E_{Fe(001)} + E_{Au(001)} - E_{Au(001)/Fe(001)}]/A, \quad (11)$$

where $E_{Au(001)/Fe(001)}$ is the total energy of the modeled interface, $E_{Fe(001)}$ is the total energy of a free Fe(001) slab, $E_{Au(001)}$ is the total energy of a free Au(001) slab, and A is the area of the interface. In Eq. (11), all the computed energies correspond to systems in which the atomic positions were fully relaxed and, for the Au(001)/Fe(001) interface and the Au(001) slab, to systems subject to the strain field induced by the PBE mismatch. In the Au(001)/Fe(001) system and in the free Fe slab, the number of Fe layers was kept fixed to 10 layers while the number of Au layers varied.

The calculated work of adhesion is presented in Fig. 9 as a function of the number of Au layers. The work of adhesion is minimum for 1 ML of Au deposited on Fe, increases strongly for 2 Au MLs, then decreases and converges to a value of $\approx$2.85 J/m^2 for slabs of more than 4 MLs. This result means that the interaction between Fe and Au at the interface is stronger for 2 MLs than for a larger number of layers. Similar behaviors were found in other interfaces with iron substrates: A much larger work of adhesion was obtained for a coating

of 1 ML in ZrC(100)/Fe(110)[45] or in TiC(100)/Fe(110).[46] The converged value of 2.85 J/m^2 is intermediate between the Fe-Fe and Au-Au intrinsic adhesions: $2\gamma_{001}^{Fe} = 4.95$ J/m^2 for Fe-Fe and $2\gamma_{001}^{Au} = 1.74$ J/m^2 for Au-Au. In addition, the work of adhesion, W_{ad}, is positive in agreement with the tendency to form core-shell Fe@Au nanoparticles.

The work of adhesion can be related to the interface energy and interface surface stress in Au by

$$\begin{aligned} W_{ad} &= [E_{Fe(001)} + E_{Au(001)} - E_{Au(001)/Fe(001)}]/A \\ &= \gamma_{001}^{Fe} + \gamma_{001}^{Au} + 2\sigma_{001}^{Au}\epsilon_{xx} - (\gamma_{int} + 2\sigma_{int}\epsilon_{xx}) \quad (12) \end{aligned}$$

using the definitions given in Eqs. (2) and (4):

$$\begin{aligned} E_{Au(001)/Fe(001)} &= N n_{at} E_{bulk}^{Au} + N' n'_{at} E_{bulk}^{Fe} + u_{el}V \\ &+ 2\sigma_{001}^{Au}\epsilon_{xx}A + \gamma_{001}^{Au}A + \gamma_{001}^{Fe}A \\ &+ \gamma_{int}A + 2\sigma_{int}\epsilon_{xx}A, \quad (13) \end{aligned}$$

where N, N', n_{at}, and n'_{at} are, respectively, the number of layers and the number of atoms per layer in the Au and Fe slabs, u_{el} is the elastic energy per unit volume in the Au slab, and γ_{int} and σ_{int} are, respectively, the interface energy and surface stress. The error made on the W_{ad} value due to the too large mismatch given by PBE compared to experiments can then be estimated. By assuming that this error is only due to the difference $\Delta\epsilon_{xx} = \epsilon_{xx}^{PBE} - \epsilon_{xx}^0$ between the PBE and the experimental strains in Au, the error ΔW_{ad} made on the W_{ad} value reads

$$\Delta W_{ad} = 2(\sigma_{001}^{Au} - \sigma_{int})\Delta\epsilon_{xx}, \quad (14)$$

which depends on how much the Au surface stress is modified by the presence of the Fe substrate. It is thus difficult to draw a clear conclusion on the effect of the PBE mismatch on the value of the Au(001)/Fe(001) work of adhesion. However, σ_{int} can be reasonably estimated to be of the order of σ_{001}^{Au}. The error done on the work of adhesion is thus of the order of $\Delta W_{ad} \approx 2\sigma_{001}^{Au}\Delta\epsilon_{xx} = 116.5$ mJ/m^2, corresponding to a relative error of $\frac{\Delta W_{ad}}{W_{ad}} = 4\%$.

On the other hand, by using the previous results of Sec. IV, the value of $\gamma_{int} + 2\sigma_{int}\epsilon_{xx}^{PBE}$ can be estimated to $\approx$571 mJ/m^2, which can be used in an attempt to understand its physical implication for the Fe@Au nanoparticles. Indeed, the core-shell Fe@Au nanoparticles which were experimentally observed exhibit Au(001) facets in epitaxy at 45° on an Fe(001) core. This geometry is quite consistent with the obtained value since, in this case, the spreading parameter $S = \gamma_{001}^{Fe} - \gamma_{int} - 2\sigma_{int}\epsilon_{xx}^{PBE} - \gamma_{001}^{Au} - 2\sigma_{001}^{Au}\epsilon_{xx}^{PBE} = 1033.8$ mJ/m^2, which takes into account both the surface excess free and elastic energy, is positive. It is hence energetically favorable to have an Fe core surrounded by a shell of gold, as observed experimentally.

To be fully consistent, the other interfaces which might be present in the Fe@Au nanoparticles, such as the Au(111)/Fe(110) one, should also be taken into account. However, in the case of the Fe nanocubes with Fe(001) facets covered by Au, the main interfaces are the Au(001)/Fe(001) ones and, if present, the Au(111)/Fe(110) interfaces would only appear at the truncated corners of the Fe nanocubes. Nevertheless, work in that direction is under progress and will be presented in a forthcoming paper.
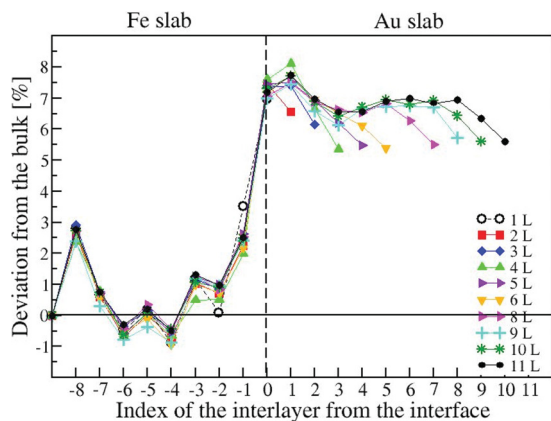
FIG. 10. (Color online) Relaxation as a percentage of the bulk interlayer distance in the Au(001)/Fe(001) interface. The relaxation is given as a percentage of the respective bulk value in each slab, Fe or Au. The index on the x axis corresponds to the position of the interlayer numbered from the interface (L in Fig. 2); see text. The different symbols denote the different numbers of Au layers.

B. Structure

In the Au(001)/Fe(001) systems, the deviation Δd of the interlayer distances from the bulk values is analyzed as a function of the position of the layers. Figure 10 reports the deviation Δd of the interlayer distances in Fe(001) and Au(001) with respect to their respective bulk values for different numbers of layers in the Au slab. The numbers on the x axis correspond to the index of the interlayer in the Fe(001)/Au(001) system, counted from the interface. The deviation of the interlayer distances with respect to the bulk one in the Fe(001) slab, Δd_{-i} (indexed as $-i$ in Fig. 10), is defined as $\Delta d_{-i} = (d_{-i,-(i+1)} - d_{\text{bulk}}^{\text{Fe}})/d_{\text{bulk}}^{\text{Fe}}$, where $d_{-i,-(i+1)}$ is the interlayer distance between the $-i$ and $-(i+1)$ iron layers numbered from the interface. Similarly, in the Au(001) slab, the deviation of the interlayer distances with respect to the bulk one, Δd_i (indexed as $+i$ in Fig. 10), is defined as $\Delta d_i = (d_{i,i+1} - d_{\text{bulk}}^{\text{Au}})/d_{\text{bulk}}^{\text{Au}}$. The deviation Δd_0 for the index 0 is defined as $\Delta d_0 = (d_0 - d_{\text{FeAu}})/d_{\text{FeAu}}$, where d_0 is the interlayer distance between the Fe and Au surfaces at the interface and d_{FeAu} is the average value between the bulk interlayer distances of Fe(001) and of Au(001): $d_{\text{FeAu}} = (a_{\text{Fe}} + a_{\text{Au}})/4 = 1.7522$ Å.

The variation of the interlayer distances in the Fe(001) slab weakly depends on the number of Au layers except for a very small number of Au layers. Starting from the bottom of the Fe slab (index -8), one observes a strong expansion which is an artefact due to the presence of the two fixed bottom layers. Then the slab interlayer distances relax around zero (index between -6 and -4) inside the slab. This is an indication that 10 layers are sufficient to converge the Fe(001) interlayer distance to its bulk value in the middle of the slab, in agreement with our analysis performed on the free Fe slab (Fig. 4). Close to the interface, the distances start to expand again and reach the value of $\approx +2.4\%$ for the interlayer distance closer to the interface (index -1). In order to unambiguously attribute this expansion to the proximity of Au atoms, we report in Fig. 11 a comparison between the evolution of the interlayer distances in the 10-layer Fe slab of the Au(001)/Fe(001) interface and
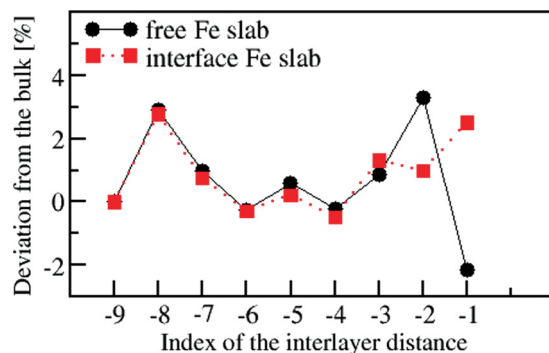

FIG. 11. (Color online) Relaxation of the interlayer distances as a percentage of the bulk interlayer spacings, as a function of the interlayer index in the Fe(001) slab (black circles) and in the Fe substrate of the Au(001)/Fe(001) interface (red squares).

those of a 10-layer free Fe slab in which 2 layers were kept fixed on one side (corresponding to index -9). The interlayer distances are very different at the interface and at the free surface (indexes from -3 to -1). For the free surface, the interlayer distance decreases by an amount of -2.2% (index -1), in agreement with the data of Fig. 4. The expansion of the Fe slab at the interface is therefore due to the proximity of the interface Au atoms, even when only one Au ML is deposited.

The evolution of the interlayer distances in the Au slab of the Au(001)/Fe(001) interface is very different than for the free relaxed Au slab (see Fig. 7). As soon as the number of layers in the Au slab is equal to or larger than 4, the same behavior is observed for all the Au slabs: The first two interlayer distances close to the interface increase by an amount of $\approx +7.8\%$ then the interlayer distances saturate around a value of $\approx +6.8\%$ and, finally, close to the free Au(001) surface, the interlayer distances expansion is smaller and becomes $\approx +5.4\%$. It should be noted that the Au slab deposited on the Fe(001) substrate at the Fe lattice parameter is subject to a significant compression in the xy plane: $\epsilon_{xx}^{\text{PBE}} = \epsilon_{yy}^{\text{PBE}} = -3.95\%$. Some of the visible effects on the Au interlayer distances are therefore due to this compression, as will be discussed later. If the system were homogeneous (without finite-size effects), this contraction in the xy plane would induce a strain in the z direction of $\epsilon_{zz} = -2C_{12}\epsilon_{xx}^{\text{PBE}}/C_{11} = +5.40\%$ [Eq. (6)]. The observed discrepancy between the calculated value of ϵ_{zz} and those extracted from the plateau at $\approx +6.8\%$ in Fig. 7 (with a large number of Au layers) is attributed to nonlinear effects: Linear elasticity theory does not hold for deformations that are too large.

Figure 12 reports the deviation of the interlayer distances from the bulk values in several 11-layer Au free slabs with different ϵ_{xx} contractions. These results are compared to the interlayer distances extracted from the 11-layer Au slab in epitaxy on the Fe(001) in the Au(100)/Fe(001) interface. The behavior of the Au slab in the Au(001)/Fe(001) interface resembles that of a free Au(001) slab subject to the same contraction in the x and y directions, except for the two closest layers to the interface (indexes 1 and 2). The interlayer distances corresponding to the slab at the PBE Au lattice parameter, a_{Au} in Table I, are shown as blue triangles (0%). As has already been shown in Fig. 7, the first layer close to the surface shows a contraction of -1.6%, but the effect of the
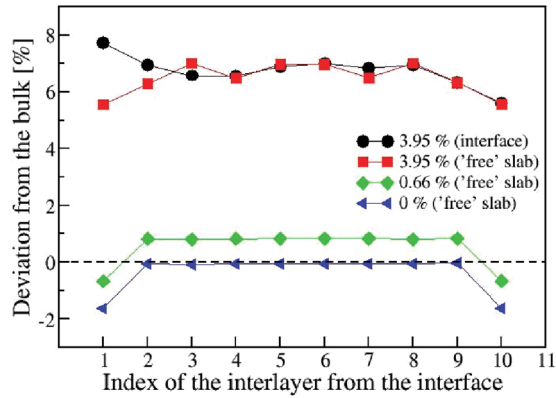
FIG. 12. (Color online) Comparison of the Au(001) interlayer distances as a percentage of the bulk interlayer distances for the Au(001)/Fe(001) interface and for Au(001) slabs computed for different ϵ_{xx} strains (see text).

surface is barely visible on the sublayers. In contrast, for the Au slab in the Au(001)/Fe(001) interface (i.e., for a ϵ_{xx} strain corresponding to the PBE mismatch, shown as black circles), the interlayer distances in the proximity of the Au/Fe interface are expanded by $\approx +7.8\%$. The corresponding Au(001) free slab with the same strain is shown as red squares and presents the same behavior, except for the two closest layers to the interface (indexes 1 and 2). This result demonstrates that the effects observed on the interlayer Au distances in the Au(001)/Fe(001) interface in Fig. 10 are elastic effects due to the PBE lattice mismatch except for the two interlayer distances closest to the interface. The observed expansion of the layers close to the interface can therefore be expected to be present even for a much smaller lattice mismatch. As a comparison, the interlayer distances one would obtain if the lattice mismatch were equal to the experimental one, i.e., $+0.66\%$, are shown in Fig. 12 as green diamonds. They are similar to those at the Au bulk lattice parameter except that they are all shifted by $\approx +0.84\%$.
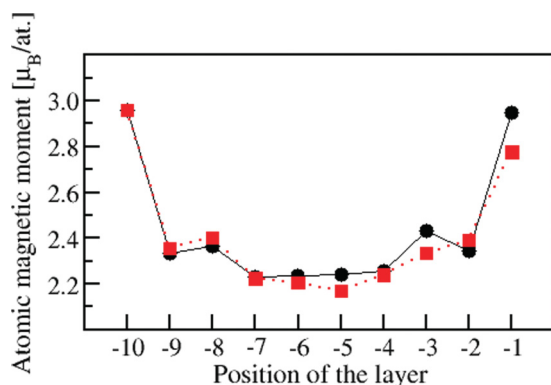

FIG. 13. (Color online) Evolution of the atomic magnetic moment of the Fe atoms as a function of the position of the layer in the Fe(001) slab (black circles) and in the Fe substrate of the Au(001)/Fe(001) interface (red squares).

C. Magnetism

Regarding the magnetic properties, Fig. 13 reports the atomic magnetic moments of the Fe atoms as a function of their position in a free Fe(001) slab (black circles) in which two layers were fixed on one side (corresponding to indexes -10 and -9) and in the Fe substrate of the Au(001)/Fe(001) interface (red squares).

The Fe atoms at the slab surface undergo a strong enhancement of their magnetic moment compared to the bulk value ($+34\%$) but this enhancement is slightly lower when the Au slab is present ($+26\%$). This magnetic enhancement at the Fe(001) slab surface is therefore not due to the change in the Fe-Fe interplanar distances but to the lack of Fe atoms in the first neighboring shell. As a consequence, in the Au slab, the atoms in the interface layer have a slight magnetic moment of 0.061 μ_B/atom due to the presence of the Fe atoms whereas, in the other Au layers, the atomic magnetic moment is equal (or very close) to zero. These results are in agreement with results of GGA DFT calculations performed on $Fe_n @ Au_m$ clusters for $n = 13$ and different values of m.[19] The same enhancement of the magnetic moment was found for Fe atoms of the interface; however, a smaller magnetic moment was observed on the Au atoms of the shell, even at the interface. In DFT calculations of Fe_m/Au_n multilayers in the same orientation,[17] the strong enhancement of the magnetic moment of the Fe interface atoms increases when the Fe slab thickness is increased. At the same time, a larger magnetic moment on the interface Au atoms is obtained for larger Fe slab thickness.

D. Electronic properties

In this section, the electronic properties of the Au(001)/Fe(001) interface system made of 10 Fe and N Au layers are investigated.

First, the system with $N = 11$ Au layers is studied, and Figs. 14(a) and 14(b) report the projected densities of the d states (PDOS) of individual Fe and Au atoms of the corresponding Au(001)/Fe(001) system. Since the s and p PDOS are much less important, they are not presented. Spin up and down are represented as positive and negative values, respectively. The PDOS of the Fe and Au atoms at three positions are shown: at the free surface, in the center (fifth layer), and in the interface layer. The PDOS for the Fe and Au atoms in the center are shown as thin black lines and are very close to the PDOS of their bulks (not shown). The effects of the free surfaces and of the interface can be seen on the PDOS represented as green lines and red lines, respectively. Comparing the PDOS of Fe atoms at the surface or at the interface with the one in the center, one observes that the presence of the surface or interface shifts the spin-down states by around $+2$ eV down to 0–0.5 eV; i.e., these states decrease in energy. This effect is slightly more pronounced for the Fe atoms at the surface than for those at the interface; however, one should recall that the Fe surface atoms are fixed at the bulk positions. In addition, due to the presence of the surface or interface, the high-energy spin-up states below the Fermi level (vertical dashed line) shift down to lower energies: This energy shift of the majority-spin states is at the origin of the magnetic moment increase of the interface Fe atoms (Fig. 13).
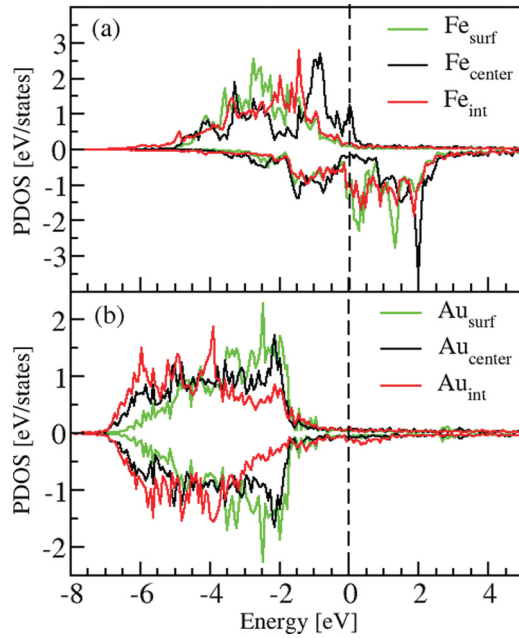
FIG. 14. (Color online) Projected densities of the d states of individual atoms in the Au(001)/Fe(001) interface with 11 Au layers. (a) Fe_{surf} denotes the fixed Fe atoms at the bottom of the Fe slab, Fe_{center} the Fe atoms in the center of the slab, and Fe_{int} the Fe atoms at the interface. (b) Au_{surf} denotes the Au atoms at the top of the Au slab, Au_{center} the Au atoms in the center of the slab, and Au_{int} the Au atoms at the interface. Spin up and down are represented as positive and negative values, respectively.

Similarly, comparing the PDOS of Au atoms at the surface or at the interface with the one in the center, one observes that the presence of a free surface shifts the low-energy states (between -7 and -5 eV) to higher energies around -2 and -4 eV. The presence of an interface induces an opposite effect: the number of high-energy states (between -2 and -4 eV) is less important than the one for Au atoms in the center of the slab. In addition, these states shift to lower energy (between

-7 and -5 eV). Remarkably, a difference between the number of spin-up and spin-down states appears around -2 eV for the Au atoms at the interface, which explains the small magnetic moment of these atoms.

The Fe and Au PDOS are subsequently analyzed as a function of the number of Au MLs, by focusing on the atoms in the vicinity of the interface. Figure 15 presents the PDOS of the Au and Fe atoms belonging to the interface (Fe_{int} and Au_{int}) and of the Au atoms just above the interface (Au_{int+1}), for Au(001)/Fe(001) systems with 2 Au MLs [Figs. 15(a) and 15(b)], with 3 Au MLs [Figs. 15(c) and 15(d)], and with 11 Au MLs [Figs. 15(e) and 15(f)].

As the number of Au MLs is increased, the PDOS of the Fe atoms at the interface, Fe_{int} [red lines in Figs. 15(a), 15(c), and 15(e)], are not considerably modified, which indicates that the presence of the interface alters the Fe atoms PDOS as soon as the first Au monolayer is deposited (not shown here). Similarly, the PDOS of the Au atoms at the interface, Au_{int} [green lines in Figs. 15(a), 15(c), and 15(e)], does not change significantly when the number of Au MLs is increased. However, the PDOS of the Au atoms just above the interface (Au_{int+1}) [light-blue lines in Figs. 15(b), 15(d), and 15(f)] is very different for the Au(001)/Fe(001) systems with only 2 Au MLs than for the ones with more Au layers. Indeed, the Au_{int+1} PDOS in Fig. 15(b) resembles that of the surface atoms in the Au slab [green line in Fig. 14(b)], whereas the Au_{int+1} PDOS in Figs. 15(d) and 15(f) look more like the interface atom one [red line in Fig. 14(b)]. As a consequence, the Au-Fe PDOS overlap is more important for the second nearest neighbors atoms, Au_{int+1} and Fe_{int}, for the system with 2 Au MLs than for the others. With an additional Au ML, i.e., for the system with 3 MLs, the Au_{int+1} PDOS becomes similar to that of the system with 11 Au MLs and the Au-Fe overlap becomes less important. The fact that the work of adhesion of the Au(001)/Fe(001) interface is larger for the system with 2 Au MLs (Fig. 9) is therefore due to a stronger bonding between the Fe interface atoms and the Au surface atoms. With additional Au MLs, the Au surface atoms and the
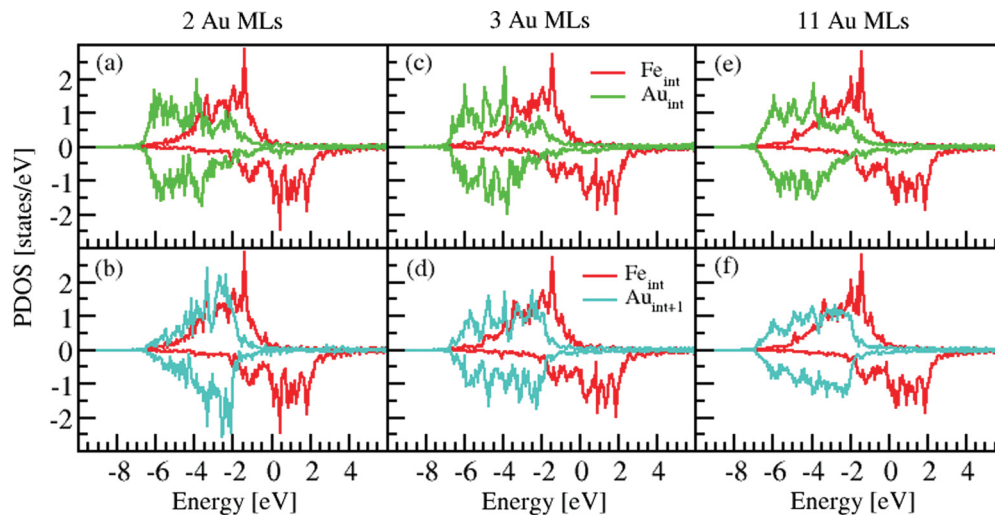

FIG. 15. (Color online) Projected densities of the d states of the Fe and Au atoms of the interface (Fe_{int}, red lines; Au_{int}, green lines) and of Au atoms of the layers above (Au_{int+1}, light-blue lines) the interface, in the Au(001)/Fe(001) system with 2 Au MLs [(a) and (b)], 3 Au MLs [(c) and (d)], and 11 Au MLs [(e) and (f)]. Spin up and down are represented as positive and negative values, respectively.
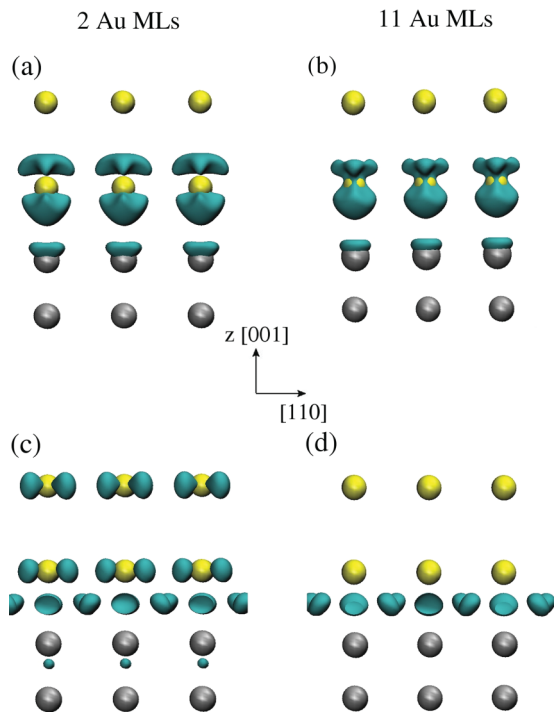
FIG. 16. (Color online) Upper graphs: Isosurfaces (in green) of negative charge density differences for (a) 2 Au MLs and (b) 11 Au MLs deposited on Fe. Lower graphs: Isosurfaces (in green) of positive charge density differences for (c) 2 Au MLs and (d) 11 MLs deposited on Fe. Au and Fe atoms are depicted in yellow and gray, respectively.

Fe interface atoms are too distant and no longer interact, which induces a reduction of the work of adhesion.

The important bonding between the interface Fe atoms and the surface Au atoms in the Au(001)/Fe(001) system with 2 Au MLs can also be observed in Fig. 16, where isosurfaces of charge density differences are shown. These isosurfaces were obtained by subtracting from the total charge density (in $e/\text{Å}^3$) of the Au(001)/Fe(001) system the total charge densities of free Fe and Au slabs, in which atoms were frozen at their positions in the Au(001)/Fe(001) system:

$$\rho_{int}(\mathbf{r}) = \rho_{Au(001)/Fe(001)}(\mathbf{r}) - \rho^*_{Au(001)}(\mathbf{r}) - \rho^*_{Fe(001)}(\mathbf{r}), \quad (15)$$

where ρ^* denotes the densities of frozen Fe and Au slabs at their positions in the interface system. The remaining negative density in $\rho_{int}(\mathbf{r})$ corresponds therefore to a deficit of electrons and the positive density to an excess of electrons, due to the presence of the interface with respect to the free Fe and Au slabs.

Isosurfaces of $\rho_{int}(\mathbf{r})$ for negative isovalues of $-0.038e/\text{Å}^3$ are shown for a gold coating of 2 MLs in Fig. 16(a) and for a gold coating of 11 MLs in Fig. 16(b). The selected isosurfaces correspond to a deficit in electrons and are well located on the Au atoms of the interface and slightly on the Fe atoms of the interface. Accordingly, the contribution to the bonding between Au(001) and Fe(001) mainly comes from electrons of the Au interface atoms.

In Fig. 16(c) and 16(d), isosurfaces of $\rho_{int}(\mathbf{r})$ for positive isovalues of $+0.033e/\text{Å}^3$ are shown for two different gold coatings of 2 and 11 MLs, respectively. In that case, the selected isosurfaces correspond to an excess of electrons in the

TABLE III. Bader atomic charges computed on selected atoms in the Au(001)/Fe(001) systems with 2 Au MLs and with 11 Au MLs.

	2 Au MLs	11 Au MLs
Fe_{center}	8.000	8.000
Fe_{int-1}	8.013	8.017
Fe_{int}	7.705	7.706
Au_{int}	11.230	11.262
Au_{int+1}	11.058	11.023
Au_{center}	—	11.000
Au_{surf}	—	11.040

Au(001)/Fe(001) system and are well located at the interface between the Au and Fe atoms. However, for the gold coating of 2 MLs, there is an important excess of charge density on the Au atoms of the interface but also on the Au surface atoms, the latter of which is not present for 11 MLs. Indeed, when additional Au MLs are deposited, the excess electronic density on the Au interface and surface atoms becomes less and less important.

This result is confirmed by computing the atomic charges, evaluated using Bader theory.[47] In Table III, the atomic charges of selected atoms in the Au(001)/Fe(001) systems with 2 Au MLs and with 11 Au MLs are presented. In the Fe slab, the center atoms bear a charge of $8.00e$, which corresponds of the number of valence electrons included in the Fe pseudopotential. In the two systems (2 Au MLs and 11 Au MLs), this value is modified close to the interface and becomes slightly larger for Fe atoms of the layer below the interface (Fe_{int-1}), whereas Fe atoms of the interface layer bear a much smaller charge of $7.706e$. In the Au slab with 11 MLs, the charge of the center atoms is equal to $11.00e$, which corresponds to the number of valence electrons included in the Au pseudopotential. In this system, the charge of the Au interface atoms is equal to $11.262e$, which is larger than that of Au center atoms, due to the charge transfer between the Fe and Au interface atoms. Au atoms above the interface (Au_{int+1}) also benefit from the charge transfer but to a much lesser extent. In comparison, the Au interface atoms in the 2-ML system bear a charge of $11.230e$, which is smaller than in the 11-ML system, but the atoms above the interface, which are also surface atoms (Au_{int+1}), exhibit a larger charge than in the 11-ML system. As observed in Fig. 16, the charge transfer from the Fe slab toward the Au one extends over the layer above the interface to a greater extent in the 2-Au-ML system than in the 11-Au-ML one. This result is consistent with the observed larger overlap between the PDOS of the Fe_{int} atoms and of the Au_{int+1} ones for the 2-ML coating [Fig. 15(b)].

The presented charge density differences and atomic charges are in agreement with the stronger work of adhesion observed for the 2-Au-ML coating. They also suggest that thin films or nanoparticles made of a Fe core (or substrate) and an Au coating of 2 MLs could exhibit peculiar properties such as enhanced catalysis, for instance, as has already been found for TiO_2[48] or FeO_x[49] with bilayer gold coatings. Work is in progress in that direction.

VI. CONCLUSION

Investigations of the structural and electronic properties of the Au(001)/Fe(001) interface as a model of core-shell

Fe@Au nanoparticles were carried out using DFT in the PBE approximation.

The calculations were set up with a careful checking of the properties of free Fe and Au slabs. In particular, the effect of the too large lattice mismatch between Au(001) and Fe(001) obtained using the PBE gradient approximation on the Au surface properties was investigated. These studies provided a reference for the investigation of the structural, magnetic, and electronic properties of the Au(001)/Fe(001) interface.

The structural properties of the Au(001)/Fe(001) interface were then analyzed in terms of the interlayer spacings for several Au coatings, from 1 to 11 MLs. It was shown that convergence of the structural and energetic properties of the interface was already achieved for Au slabs of 4 MLs. An expansion of the interlayer distances at the interface was observed in the Fe slab as well as in the Au slab. In the latter, the elastic effects due to the too large PBE mismatch were analyzed in detail.

At the interface, the magnetic moment of the Fe atoms shows a strong enhancement, although it is slightly lower than the enhancement observed for surface atoms in the free Fe slab. Additionally, the Au atoms of the interface exhibit a nonzero but very small magnetic moment.

The calculated work of adhesion presents a larger value for an Au coating of 2 MLs and then converges rapidly toward a value of 2.85 J/m^2, which, in a first approximation, gives a value for the interface energy of $\approx$571 mJ/m^2, by taking into account the surface stress on the interface. The elastic effects on the interface energy were taken into account and this allowed us to estimate the error made on the value of the work of adhesion due to the too large PBE mismatch at $\approx$4%.

The evolution of the work of adhesion as a function of the number of Au MLs was understood from the analysis of the projected electronic densities of states and the charge density differences. Indeed, a strong overlap between the electronic density of the Fe interface atoms and that of the Au surface atoms was observed for an Au coating of 2 MLs. This result indicates that the bonding of Au bilayers on the Fe(001) substrate is considerably stronger than for thicker Au coatings, but it also suggests that Fe nanocubes coated with Au bilayers could display enhanced electronic activity.

In conclusion, the calculated interface energy could explain the formation of the observed core-shell Fe@Au nanoparticles made of an Fe nanocube with Fe(001) facets surrounded by Au(001) in epitaxy at 45° on the cube facets. These recently synthesized nanoparticles present an interesting morphology and remarkable characteristics such as a magnetic core with a large magnetic moment. Moreover, they are unlikely to be oxidized.[19] Hence we expect them to be biocompatible and to be good candidates for biomedical applications.

*Corresponding author: mbenoit@cemes.fr

†Present address: MATEIS, INSA Lyon, 7, Avenue Jean Capelle, 69621 Villeurbanne Cedex, France.

[1] D. Kim, Y. Zhang, J. Kehr, T. Klason, B. Bjelke, and M. Muhammed, J. Magn. Magn. Mater. **225**, 256 (2001).

[2] T. Neuberger, B. Schöpf, H. Hofmann, M. Hofmann, and B. von Rechenberg, J. Magn. Magn. Mater. **293**, 483 (2005).

[3] H.-Y. Park, M. Schadt, L. Wang, S. Lim, P. Njoki, S. Kim, M.-Y. Jang, J. Luo, and C.-J. Zhong, Langmuir **23**, 9050 (2007).

[4] M.-C. Daniel and D. Astruc, Chem. Rev. **104**, 293 (2003).

[5] M. Chen, S. Yamamuro, D. Farrell, and S. Majetich, J. Appl. Phys. **93**, 7551 (2003).

[6] Z. Ban, Y. Barnakov, L. Feng, V. Golub, and J. O'Connor, J. Mater. Chem. **15**, 4660 (2005).

[7] S. Zhang, W. Li, C. Li, and J. Chen, J. Phys. Chem. B **110**, 24855 (2006).

[8] I. Chiang and D.-H. Chen, Adv. Funct. Mater. **17**, 1311 (2007).

[9] S.-J. Cho, S. Kauzlarich, J. Olamit, K. Liu, F. Grandjean, L. Rebbouh, and G. Long, J. Appl. Phys. **95**, 6804 (2004).

[10] E. Carpenter, J. Magn. Magn. Mater. **225**, 17 (2001).

[11] J. Lin, W. Zhou, A. Kumbhar, J. Wiemann, J. Fang, E. Carpenter, and C. O'Connor, J. Solid State Chem. **159**, 26 (2001).

[12] S.-J. Cho, A. Shahin, G. Long, J. Davies, K. Liu, F. Grandjean, and S. Kauzlarich, Chem. Mater. **18**, 960 (2006).

[13] W.-S. Chang, J.-W. Park, V. Rawat, T. Sands, and G. Lee, Nanotechnology **17**, 5131 (2006).

[14] K. Sato, B. Bian, and Y. Hirotsu, Jpn. J. Appl. Phys. **41**, L1 (2002).

[15] A. Naitabdi, L. K. Ono, F. Behafarid, and B. R. Cuenya, J. Phys. Chem. C **113**, 1433 (2009).

[16] Experimental results will be presented elsewhere.

[17] M. Sternik and K. Parlinski, Phys. Rev. B **75**, 212406 (2007).

[18] C. M. Fang, R. A. de Groot, M. M. J. Bischoff, and H. van Kempen, Phys. Rev. B **58**, 6772 (1998).

[19] Q. Sun, A. K. Kandalam, Q. Wang, P. Jena, Y. Kawazoe, and M. Marquez, Phys. Rev. B **73**, 134409 (2006).

[20] W. Kohn and L. J. Sham, Phys. Rev. **140**, A1133 (1965).

[21] J. Hafner, Acta Mater. **48**, 71 (2000).

[22] P. K. Nandi, M. C. Valsakumar, S. Chandra, H. K. Sahu, and C. S. Sundar, J. Phys.: Condens. Matter **22**, 345501 (2010).

[23] A. Dewaele, M. Torrent, P. Loubeyre, and M. Mezouar, Phys. Rev. B **78**, 104102 (2008).

[24] C. Domain and C. S. Becquart, Phys. Rev. B **65**, 024103 (2001).

[25] C. Kittel, *Introduction to Solid State Physics*, 6th ed. (Wiley, New York, 1986).

[26] T. Tsuchiya and K. Kawamura, J. Chem. Phys. **116**, 2121 (2002).

[27] H. L. Zhang, S. Lu, M. P. J. Punkkinen, Q.-M. Hu, B. Johansson, and L. Vitos, Phys. Rev. B **82**, 132409 (2010).

[28] J. R. Neighbours and G. A. Alers, Phys. Rev. **111**, 707 (1958).

[29] D. Isaak and K. Masuda, J. Geophys. Res. **100**, 17689 (1995).

[30] P. Söderlind, O. Eriksson, J. M. Wills, and A. M. Boring, Phys. Rev. B **48**, 5844 (1993).

[31] H. C. Hsueh, J. Crain, G. Y. Guo, H. Y. Chen, C. C. Lee, K. P. Chang, and H. L. Shih, Phys. Rev. B **66**, 052420 (2002).

[32] N. E. Singh-Miller and N. Marzari, Phys. Rev. B **80**, 235407 (2009).

[33] W. Tyson and W. Miller, Surf. Sci. **62**, 267 (1977).

[34] F. R. De Boer, R. Boom, W. C. M. Mattens, A. R. Miedema, and A. K. Niessen, *Cohesion in Metals: Transition Metal Alloys*, Cohesion and Structure, Vol. 1 (North-Holland, Amsterdam, 1989).

[35] A. R. Miedema, Z. Metallkde. **69**, 287 (1978).

[36] M. Eder, K. Terakura, and J. Hafner, Phys. Rev. B **64**, 115426 (2001).

[37] M. J. Spencer, A. Hung, I. K. Snook, and I. Yarovsky, Surf. Sci. **513**, 389 (2002).

[38] M. Escaño, H. Nakanishi, and H. Kasai, J. Phys: Condens. Matter **19**, 482002 (2007).

[39] P. Błoński and A. Kiejna, Surf. Sci. **601**, 123 (2007).

[40] H. Shi and C. Stampfl, Phys. Rev. B **77**, 094127 (2008).

[41] V. Zólyomi, L. Vitos, S. K. Kwon, and J. Kollár, J. Phys.: Condens. Matter **21**, 095007 (2009).

[42] P. Müller and A. Saúl, Surf. Sci. Rep. **54**, 157 (2004).

[43] Y. Umeno, C. Elsaesser, B. Meyer, P. Gumbsch, M. Nothacker, J. Weissmueller, and F. Evers, Europhys. Lett. **78**, 13001 (2007).

[44] M. I. Haftel and K. Gall, Phys. Rev. B **74**, 035420 (2006).

[45] A. Arya and E. A. Carter, Surf. Sci. **560**, 103 (2004).

[46] A. Arya and E. A. Carter, J. Chem. Phys. **118**, 8982 (2003).

[47] R. F. W. Bader, *Atoms in Molecules - A Quantum Theory* (Oxford University Press, Oxford, 1990).

[48] M. Chen and D. Goodman, Science **306**, 252 (2004).

[49] A. Herzing, C. Kiely, A. Carley, P. Landon, and C. Hutchings, Science **321**, 1331 (2008).